Journal of the Korean Astronomical Society
53: 69 ∼ 75, 2020 June

https://doi.org/10.5303/JKAS.2020.53.3.69
pISSN: 1225-4614 · eISSN: 2288-890X
http://jkas.kas.org

Sun Flux Variations Due to Orbiting planets: The Solar System as a Non-compact Planetary System

Hugo Barbier[1], Ericson D. López[1,2], Bryan Tipán[1], and Christian L. Vásconez[1]

[1]Departamento de Física, Escuela Politécnica Nacional, Quito, Ecuador; hugo.barbier@epn.edu.ec, christian.vasconez@epn.edu.ec

[2]Observatorio Astrónomico de Quito, Escuela Politécnica Nacional, Quito, Ecuador; ericsson.lopez@epn.edu.ec

Received September 21, 2019; accepted May 4, 2020

Abstract: We study the photometric phase curves for the planets of our solar system which can be considered as a prototypical non-compact planetary system. We focus on modeling the small variations caused by three effects: reflection, ellipsoidal, and Doppler beaming. Theoretical predictions for these photometric variations are proposed, considering a hypothetical external observer. Unlike similar studies of multi-planetary systems, the physical and geometrical parameters for each planet of the solar system are well-known. Therefore, we can accurately evaluate the relationships that shape the planetary light curves for a fictitious external observer. Our results suggest that, for all planets, the ellipsoidal effect is very weak while the Doppler beaming effect (DBE) is, in general, dominant. In fact, the DBE seems to be the principal cause of variations of the light curves for the planets of the solar system. However, for Mercury and Venus the Doppler beaming and reflection effects have similar amplitudes. The phase curves obtained for the planets of the solar system show new interesting features of interest for the study of other non-compact planetary systems.

Key words: planets and satellites: fundamental parameters — methods: numerical

1. Introduction

Since the discovery of the first exoplanet orbiting a main sequence star, Pegasi-51b, in 1995 (Mayor & Queloz 1995), the number of known exoplanets has continuously increased. Especially due the *Kepler* mission (Borucki et al. 2010), this number raised to 4040 in September 2019, including 684 multi-planet systems.[1] The NASA exoplanet archive contains 1715 confirmed planets in multi-planet systems with two or more planets, including 1043 in systems with more than two planets. Prominent examples are Kepler-11, with 6 known planets (Gelino & Kane 2014), TRAPPIST-1 (Gillon et al. 2017), and KOI-351 (alias Kepler-90), with 8 planets (Schmitt et al. 2014; Cabrera et al. 2013; Shallue & Vanderburg 2017). All of these planetary systems were found with the transit method (Borucki & Summers 1984). Some multi-planet systems detected with the radial velocity method (Mayor & Queloz 1995) are: HD-10180, which is estimated to have 6 to 9 planets (Lovis et al. 2011; Tuomi 2012), and HD-219134 with 6 planets (Gelino & Kane 2014). Thanks to the forthcoming new generation of highly sensitive space instruments and sophisticated data-analysis techniques, it is expected that the number of detected extrasolar planets will rapidly increase in the coming years, even in well-known planetary systems.

It is commonly accepted that the Doppler beaming effect (DBE) is negligible compared to the reflection and ellipsoidal effects (Esteves et al. 2013). With this in mind, our work is focused on studying the phase curves of non-compact systems. We compute the "tiny" photometric variations caused by the reflection, ellipsoidal and the Doppler beaming effects. We use data for the closest non-compact system, i.e., our own solar system. For this system, we know the physical and geometric parameters needed to evaluate the strength of each photometric effect. Special attention should be paid to non-transit configurations which are the norm for a non-compact system. Due to the applied detection methods, most of the discovered multi-planetary systems are very compact, and the probability for a single or multiple transits increases with increasing compactness of the system (Borucki & Summers 1984).

This paper is organized as follows. Section 2 briefly reviews the characteristics of the solar system. In Section 3, we present the relationships that model the reflection, ellipsoidal and Doppler beaming effects, for the eight planets of the Solar System, considering a fictitious observer located outside the system in the ecliptic plane. The results and the data analysis are summarized in Section 4. Section 5 provides a final discussion and conclusions.

2. The Solar System

For our study, we analyze the eight solar system planets: Mercury, Venus, Earth, Mars, Jupiter, Saturn, Uranus, and Neptune. We do not consider trans-Neptunian objects or small solar system bodies, due to their negligible effects on the global system dynamics. Table 1 presents the parameters used to evaluate the phase curves of the planets. Complementary, Table 2 includes some average physical values related to the Sun. Data from Tables

Corresponding author: H. Barbier

[1]See, e.g., http://exoplanetarchive.ipac.caltech.edu

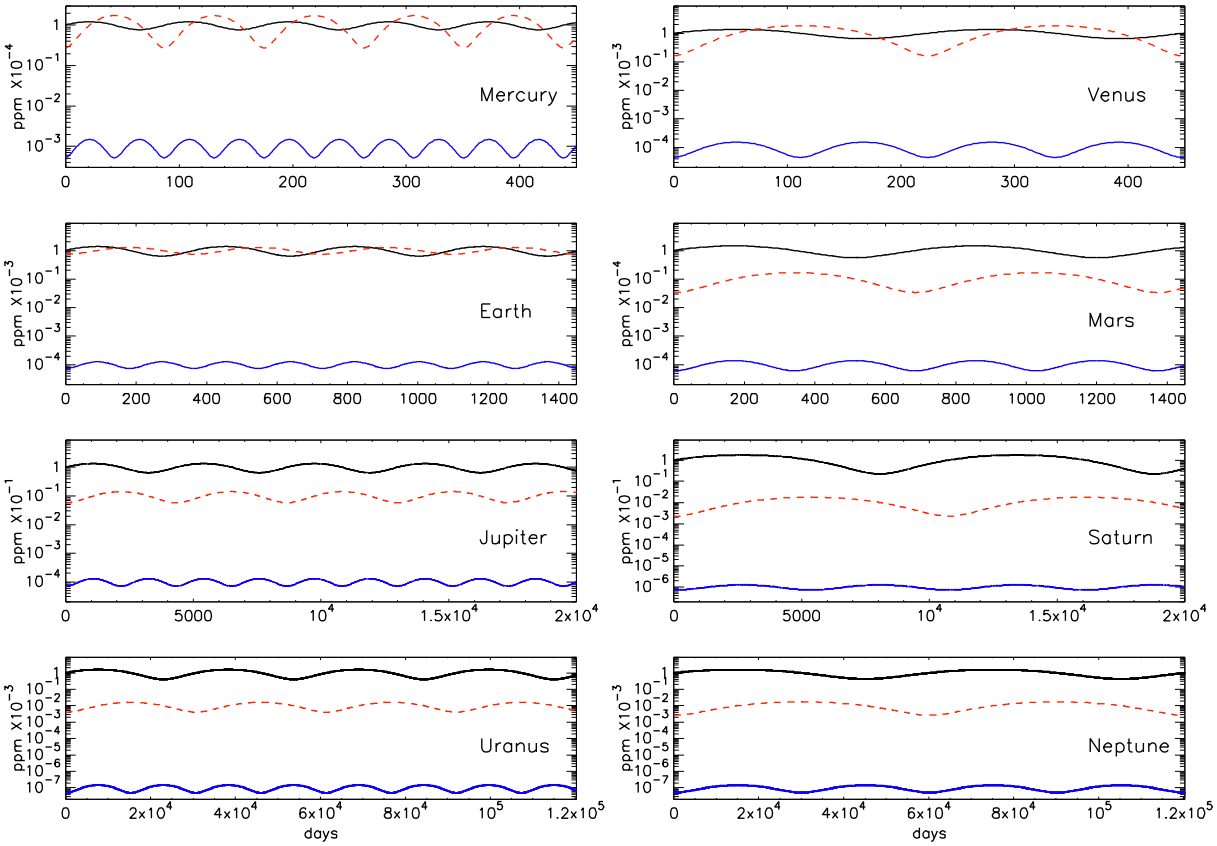

Figure 1. Logarithmic relative flux variation ($\Delta F/F_0$) as function of time for the eight planets of the solar system. Plots in each row span different time windows to improve the visualization. The black solid line corresponds to the DBE, the red dashed line to the reflection effect and the blue solid line to the ellipsoidal effect. The ellipsoidal effect is always the weaker effect.

1 and 2 reflect the fact that our planetary system is clearly a non-compact planetary system.

The Solar System can be compared to a compact system like Kepler-11, which has 6 planets concentrated in a radius of ~ 0.250 au around the host star (Gelino & Kane 2014), or with TRAPPIST-1, with 7 planets within ~ 0.063 au (Gillon et al. 2017). Planets in multi-planetary *Kepler* systems are supposed to move on quasi-circular orbits Lissauer et al. (2012). High orbit eccentricities in a multi-planetary system can have various causes such as migration (e.g., Hamers et al. 2017; Tremaine & Zakamska 2004), capture (e.g., Yu & Tremaine 2001), dissipation (in/out star) (e.g., Laskar et al. 2012; Jurić & Tremaine 2008), and the presence of a hot Jupiter with enough mass to disturb the orbits of neighboring planets (e.g., Batygin et al. 2016). Eccentricity may be an important diagnostic for the physical state of planetary systems, as highlighted by the possible anti-correlation between exoplanet eccentricities and the multiplicity of planetary systems (e.g., Zinzi & Turrini 2018; Limbach & Turner 2015).

In the case of our solar system, the orbital eccentricities e are relatively weak, except for Mercury ($e \sim 0.206$). Furthermore, the orbits are quasi-coplanar with the only exception, once again, being Mercury which has an orbit inclination of $\sim 7.005°$ with respect to the ecliptic plane. For the solar system planets, orbital periods P vary from 88 days (Mercury) to 165 years (Neptune); in compact multi-planetary systems, P is commonly few days (Gelino & Kane 2014; Gillon et al. 2017). The location of habitable zones depends on the type of the host star; its distance from the host star increases with stellar luminosity (Borucki & Summers 1984; Serrano et al. 2018).

3. THEORETICAL LIGHT-CURVE VARIATION

Ground and space-based observations measure and analyze the light curves of different multi-star and multi-planetary systems. The two predominant effects in light-curve profiles are the widely known reflection and ellipsoidal effects. More recently, the Doppler beaming effect (DBE) has been observed for eclipsing binaries (Hills & Dale 1974) and exoplanetary systems (Mazeh et al. 2012; Faigler et al. 2012). The DBE is known to have a very low intensity relative to the other effects (Loeb & Gaudi 2003; Zucker et al. 2007) and was first detected by the *CoRot* and *Kepler* space observatories.

A rotating planet orbiting a star will be subject to both tidal and rotational forces which distort the shape of the planet. Since the gravitational potential due to the star varies inversely with distance, the resulting gradient across the discrete boundaries of the

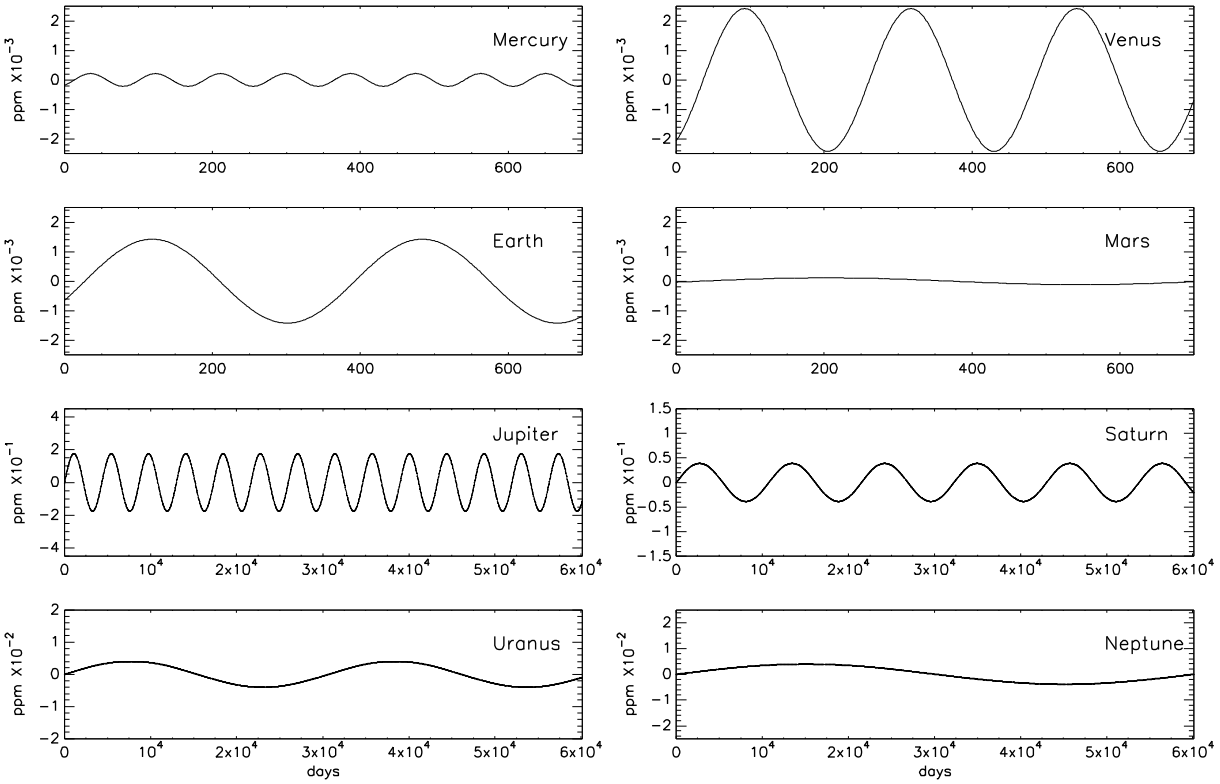

Figure 2. The direct sum of the three effects that contribute to the total $(\Delta F/F_0)_{tot}$ for each planet. The time window for the terrestrial planets corresponds to one period of Mars. One period of Neptune is used for the outer planets.

orbiting planet will induce a symmetric tidal bulge in the direction of the tide-inducing body that will deform the object into a prolate ellipsoid. Changes in the reflectivity of a planet due to surface features, oblateness, climate, etc. have a relative strength at the level of parts per billion (ppb). Exoplanet oblateness and obliquity would also induce spin precession that under certain conditions could yield detectable signals for certain gas giants (Carter & Winn 2010). However, in the case of the solar system planets, these effects are negligible. Early estimates of a detectable variation in transit depth within a light curve due to oblateness yielded results which even for the most favorable scenarios were very close to observational limits (Seager & Hui 2002; Barnes & Fortney 2003).

In addition, there are several factors that affect the weather on a planet: axis tilt (which causes the seasons), the shape of its orbit around the star, the presence or absence of a significant atmosphere, and its average distance from the star. Important variations in temperature, weather and climatic conditions, in different places around a planet, lead to little variation in a planet's overall climate. Thus, planetary climate is not considered an appreciable flux-variation factor. Large variations in temperature could occur on tidally locked planets, but there is no such the case in our solar system. Surface and atmospheric characteristics of a planet are considered in its geometric albedo (e.g., Alberti et al. 2017); the geometric albedo of the Earth is 0.367 (de Pater 2002). We elaborate further on this in Section 3.3 where the planet reflectivity is computed through the planetary albedo.

In the following subsections, we briefly describe the Doppler beaming, ellipsoidal and reflection photometric effects.

3.1. Planetary Doppler-beaming Effect

Loeb & Gaudi (2003) were the first to suggest a new description of extrasolar-system light curves, taking into account the Doppler-beaming effect (DBE). They noted that the DBE leads to small flux variations that can be measured by sensitive *Kepler*-like telescopes (Rybicki & Lightman 2008). The observed normalized flux variability $(\Delta F/F_0)$ oscillates on time-scales close to the planetary orbital period P like

$$\frac{\Delta F}{F_0} = A_d \sin(\phi) \tag{1}$$

where F_0 is the mean intrinsic stellar flux, A_d is the DBE amplitude, and ϕ is the orbital phase angle. We set $\phi = 0$ for the inferior conjunction and $\phi = \pi$ for the superior one. The amplitude A_d follows from a Lorentz transformation of the radiated energy. For non-relativistic velocities, the observed flux F relates to the radial velocity V_r (Zucker et al. 2007; Rybicki & Lightman 2008) like

$$F = F_0 \left(1 + 4\frac{V_r}{c}\right) \tag{2}$$

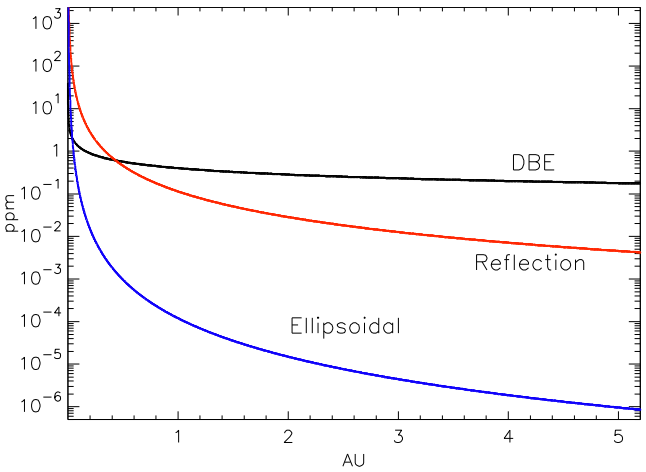

Figure 3. Decay of the amplitude of each effect for a Jupiter-type planet, as function of distance to the host star a. The black line represents the DBE (A_d), the red line is the reflection effect (A_r), and the blue line is the ellipsoidal effect (A_e). Outward of ~ 0.5 au the beaming effect is dominant. The amplitude of the beaming effects scales as $a^{-1/2}$, the reflection effect scales as a^{-2}, and the ellipsoidal effect as a^{-3}.

where c is the speed of light. If the emission is isotropic in the source rest-frame, the flux transforms in the same way as the specific intensity, resulting in a power-law spectrum. For a band-pass centered on a frequency ν_0, the normalized flux can be expressed as

$$\frac{\Delta F}{F_0} = (3 - \alpha_d)\frac{V_r}{c} \tag{3}$$

where α_d is the beaming average spectral index around ν_0 (Loeb & Gaudi 2003; Zucker et al. 2007). From the data for the Sun (see Table 2), we found $\alpha_d = -1.2211$ at a frequency $\nu_0 \sim 5 \times 10^{14}$ Hz.

The radial velocity can be expressed using its semi-amplitude K like $V_r = K\sin(\phi)$ and with

$$K = \left(\frac{2\pi G}{P_{orb}}\right)^{1/3}\left[\frac{M_p \sin(i)}{M_J}\right]\left(\frac{M_*}{M_\odot}\right)^{-2/3}; \tag{4}$$

where G is the gravitational constant, P_{orb} is the orbital period, i is the orbital inclination with respect to the plane of observation, and M_p, M_J, M_*, and $M_\odot$ are the masses of the planet, Jupiter, host star, and the Sun, respectively. In this case

$$\frac{\Delta F}{F_0} = (3-\alpha_d)\frac{V_r}{c} = (3-\alpha_d)\frac{K\sin(\phi)}{c} = A_d \sin(\phi). \tag{5}$$

For convenience, we will use A_d in units of parts per million (ppm),

$$A_d = 0.67(3-\alpha_d)\left(\frac{M_*}{M_\odot}\right)^{-2/3}\left(\frac{P_{orb}}{\text{day}}\right)^{-1/3}\left(\frac{M_p \sin(i)}{M_J}\right). \tag{6}$$

3.2. Planetary Ellipsoidal Effect

A periodic deformation of the visible area of a star from the point of view of a static observer is referred to as ellipsoidal effect (Mazeh et al. 2012; Faigler et al. 2012; Welsh et al. 2010). In general, it is detected when a massive planet, like a hot Jupiter, orbits close to its host star and causes a deformation of the star due to tides. Both the emitted and the observed fluxes reach a maximum when the line of sight and the line connecting star and planet are perpendicular.

The relative flux variation due to the ellipsoidal effect oscillates with a period of $P/2$ like

$$\frac{\Delta F}{F_0} = A_e \cos(2\phi) \tag{7}$$

where A_e is the amplitude of this variation. In particular, A_e is affected by the linear (u) and gravitational (y) darkening limbs (Esteves et al. 2013; Loeb & Gaudi 2003) and can be written as

$$A_e = \alpha_e \frac{M_p}{M_*}\left(\frac{R_*}{a}\right)^3 \sin^2(i) \tag{8}$$

where $\alpha_e = 0.15(15+u)(1+y)/(3-u)$, a is the semi-major axis of the planet orbit and R_* is the stellar radius. For the Sun, $u = 0.32$ (Cox 2000) and $y = 0.45$ (Loeb & Gaudi 2003).

As we did for the DBE, we rewrite the amplitude of the ellipsoidal effect in ppm units,

$$A_e = 12.8\alpha_e \sin(i)\left(\frac{R_*}{a}\right)^3\left(\frac{M_*}{M_\odot}\right)^{-2}\left(\frac{P_{orb}}{\text{day}}\right)^{-2}. \tag{9}$$

3.3. Planetary Reflection Effect

The flux due to radiation reflected by a planet oscillates with a period P_{orb} like

$$\frac{\Delta F}{F_0} = A_r \cos(\phi) \tag{10}$$

where A_r is the reflection amplitude. The amplitude A_r is related to the planetary radius R_p and to the geometric albedo A_{geo} like

$$A_r = A_{geo}\left(\frac{R_p}{a}\right)^2 \sin(i) \tag{11}$$

or in ppm units,

$$A_r = 570 A_{geo}\sin(i)\left(\frac{M_*}{M_\odot}\right)^{-2/3}\left(\frac{P_{orb}}{\text{day}}\right)^{-4/3}\left(\frac{R_p}{R_J}\right)^2 \tag{12}$$

where R_J is the radius of Jupiter. Estimates of A_{geo} can be used to infer some atmospheric or surface characteristics of the planet (e.g., Alberti et al. 2017).

The *total* fractional variability of the flux, $(\Delta F/F_0)_{tot}$, can be computed directly as a linear combination of the three photometric effects like

$$\left(\frac{\Delta F}{F_0}\right)_{tot} = A_d \sin(\phi) - A_e \cos(2\phi) - A_r \cos(\phi) \tag{13}$$

Table 1
Solar system planets parameters (Cox 2000)

Planet	P (yr)	e	i	M_p (M_j)	R_p (au)	a (au)	Ag
Mercury	2.41×10^{-1}	2.06×10^{-1}	83.00	1.73×10^{-4}	1.63×10^{-5}	3.87×10^{-1}	0.10
Venus	6.15×10^{-1}	6.77×10^{-3}	86.61	2.56×10^{-3}	4.05×10^{-5}	7.23×10^{-1}	0.67
Earth	1.00	1.67×10^{-2}	90.00	3.14×10^{-3}	4.26×10^{-5}	1.00	0.37
Mars	1.88	9.34×10^{-2}	88.15	3.36×10^{-4}	2.27×10^{-5}	1.52	0.15
Jupiter	1.19×10^{1}	4.84×10^{-2}	88.69	1.00	4.67×10^{-4}	5.20	0.52
Saturn	2.94×10^{1}	5.42×10^{-2}	87.52	2.99×10^{-1}	3.89×10^{-4}	9.58	0.47
Uranus	8.40×10^{1}	4.72×10^{-2}	89.23	4.40×10^{-2}	1.70×10^{-4}	1.92×10^{1}	0.51
Neptune	1.65×10^{2}	8.59×10^{-3}	88.23	5.35×10^{-2}	1.65×10^{-4}	3.01×10^{1}	0.41

where $\phi = 0$ corresponds to the primary eclipse (transit) and $\phi = \pi$ to the secondary eclipse (occultation). When the planet leaves the transit, all three photometric effects give a positive contribution to the variation of the total flux.

4. Results

Figure 1 shows the strengths of the DBE, reflection, and ellipsoidal photometric effects for each planet of the solar system as function of time. The strongest combined effect can be seen for Jupiter with $\Delta F/F_0 \approx 1.75 \times 10^{-7}$ (see Table 3). For all planets, the Doppler-beaming and reflection effects are dominant; for Mercury, Venus, and the Earth, they are also of the same order. For all planets, the ellipsoidal effect is weaker than the other effects by several orders of magnitude. Furthermore, the ellipsoidal effect rapidly becomes weaker with increasing distance from the star; this fact could be used as a compactness criterion. The amplitude of the ellipsoidal effect scales as a^{-3}, the reflection effect as a^{-2}, and the Doppler-beaming effect as $a^{-1/2}$.

We note that the technology necessary to observe such tiny amplitudes is not yet available. Nevertheless, recent works have successfully modeled planetary phase variations close to the noise level ($\sim 10^{-6}$) using *Kepler* space telescope data (e.g., Esteves et al. 2015).

Figure 2 shows the cumulative contribution of the three effects to the phase curve for each of the solar planets. The curves are plotted for fixed time windows corresponding to the orbital period of Mars for the terrestrial planets and to the period of Neptune for the outer planets. A comparison of these composite phase curves confirms that the DBE is the predominant effect for the outer planets, while DBE and reflection effect are of equal importance for the inner planets. Table 3 shows the maximum values of the photometric amplitudes A_d, A_e, and A_r for each solar system planet.

For compact systems, it is expected that the reflection and ellipsoidal effects dominate over the DBE. However, as can be seen in Figure 3, for a Jupiter-type planet located $\lesssim 0.5$ au away from its host star the beaming effect is dominant. It is thus reasonable to suppose that the ellipsoidal effect will be weak for the outer planets of a non-compact planetary systems. Again, this is consistent with the observations for the solar system planets except Mercury.

Our results suggest that the variations of the total flux of the Sun due to orbiting planets is on the order of $\sim 10^{-7}$ or less. Such a small variation cannot be observed with current technology. However, this may change with future missions like PLATO (ESA-SCI) (Rauer et al. 2014).

5. Discussion and Conclusions

As the detection of large planets located close to their host stars is more likely than for other combinations of distance and mass, discovered planetary systems are usually compact. They have ellipsoidal and reflection photometric amplitudes larger than the Doppler beaming amplitude.

In this study, we have evaluated the phase curves for the eight planets of the Solar System. The tiny variations of the stellar flux due to the Doppler beaming, reflection, and ellipsoidal effects have been studied from the point of view of a fictitious observer located outside of this non-compact system but aligned with the ecliptic plane. The contributions by individual effects were analyzed to better understand the effects expected for non-compact systems.

To date, exoplanet studies do not take into account stellar flux fluctuations smaller than ~ 10 ppm (Esteves et al. 2013) in relative terms. This is directly related to the sensitivity limitations of the currently available space instruments. The *Kepler* mission achieved a photometric precision of about 50 ppm over six hours for a 12th magnitude target. This is not sufficient to detect the tiny light curve fluctuations expected from our analysis of the solar system. Even missions like CHEOPS are limited to accuracies of 150 ppm per minute for a 9th magnitude target, corresponding to 10 ppm in 6 hours of integration (Broeg et al. 2013). In general, for the brightest stars the precision is limited by a systematic noise floor of about 60 ppm in one hour of integration. For the recently launched TESS mission, the photometric precision for a 10th magnitude star is estimated to be about 200 ppm in 1 hour (Ricker et al. 2014). PLATO will reach 27 ppm in 1 hour for an 11th magnitude star, and 10 ppm for a 6th magnitude star.

The photometric signals computed in this work (Table 3) fall within the current background noise levels, and a reliable detection should occur on a confidence level of at least 5σ. Algorithms allowing to extract

Table 2
Sun parameters (Cox 2000)

$T_\odot$ (K)	$R_\odot$ (AU)	u	y
5778	4.65×10^{-3}	0.32	0.45

Table 3
Maximum light-curve variations for the solar system planets

Planet	A_d	A_e	A_r
Mercury	1.13×10^{-10}	3.51×10^{-13}	1.81×10^{-10}
Venus	1.20×10^{-9}	8.06×10^{-13}	2.10×10^{-9}
Earth	1.26×10^{-9}	3.75×10^{-13}	6.66×10^{-10}
Mars	1.09×10^{-10}	1.13×10^{-14}	3.32×10^{-11}
Jupiter	1.75×10^{-7}	8.46×10^{-13}	4.19×10^{-9}
Saturn	3.87×10^{-8}	4.05×10^{-14}	7.76×10^{-10}
Uranus	4.02×10^{-9}	7.39×10^{-16}	3.96×10^{-11}
Neptune	3.89×10^{-9}	2.34×10^{-16}	1.23×10^{-11}

signals from noisy data are in development. The strong point of these algorithms is their ability to reduce impact of correlated noise. They consider that correlated noise alters the values of all illuminated detector pixels. By looking at inter-pixel correlations, it should be possible to identify and eliminate the correlated noise.

The space instruments that provide us with data have been designed to operate no longer than a few years (four to six years for PLATO), whereas Jupiter requires 11 years for a full orbit. Thus even future instruments will not able to detect signals like those that we have predicted for the solar system planets. The community efforts need to be focused beyond the comprehension of the oscillations of the star and the influence of the stellar spots, active regions, granulation, and activity, in general rather than the short-time instrumental evolution (Hippke & Angerhausen 2015).

One of the most important conclusions of this study is that, for a hypothetical observer outside the solar system, the Doppler-beaming effect is the most relevant. This effect is the easiest one to be detected, especially for the outer planets. This is important because the DBE permits to obtain a good estimate of the planet mass from the radial velocity. The contribution of the reflection effect is appreciable, and dominant, for the inner planets. The ellipsoidal effect is practically negligible for the eight planets of our system. These results could be considered as characteristic for a non-compact system.

Despite the non-detectability of the tiny signal expected for the planets of the solar system, our work qualitatively characterizes a non-compact system and facilitates the understanding of its photometric properties, providing some insights for studies of other planetary systems.

ACKNOWLEDGMENTS

H.B. was partially supported by Escuela Politécnica Nacional project PII-DFIS-01-2018. C.L.V. acknowledges support from Escuela Politécnica Nacional projects PII-DFIS-2019-01 and PII-DFIS-2019-04.

REFERENCES

Alberti, T., Carbone, V., Lepreti, F., & Vecchio, A. 2017, Comparative Climates of the Trappist-1 Planetary System: Results from a Simple Climate-vegetation Model, ApJ, 844, 19

Barnes, J. W. & Fortney, J. J. 2003, Measuring the Oblateness and Rotation of Transiting Extrasolar Giant Planets, ApJ, 588, 545

Batygin, K., Bodenheimer, P. H., & Laughlin, G. P. 2016, In Situ Formation and Dynamical Evolution of Hot Jupiter Systems, ApJ, 829, 114

Borucki, W. J., Koch, D., Basri, G., et al. 2010, Kepler Planet-detection Mission: Introduction and First Results, Science, 327, 977

Borucki, W. J. & Summers, A. L. 1984, The Photometric Method of Detecting other Planetary Systems, Icarus, 58, 121

Broeg, C., Fortier, A., Ehrenreich, D., et al. 2013, CHEOPS: A Transit Photometry Mission for ESA's Small Mission Programme, EPJ Web Conf., 47, 03005

Cabrera, J., Csizmadia, Sz., Lehmann, H., et al. 2013, The Planetary System to KIC 11442793: a Compact Analogue to the Solar System, ApJ, 781, 18

Carter, J. A. & Winn, J. N. 2010, The Detectability of Transit Depth Variations due to Exoplanetary Oblateness and Spin Precession, ApJ, 716, 850

Cox, A. N. (ed.) 2000, Allens Astrophysical Quantities (Berlin: Springer)

Esteves, L. J., De Mooij, E. J. W., & Jayawardhana, R. 2013, Optical Phase Curves of Kepler Exoplanets, ApJ, 772, 51

Esteves, L. J., Mooij, E. J. W. D., & Jayawardhana, R. 2015, Changing Phases of Alien Worlds: Probing Atmospheres of Kepler Planets with High-precision Photometry, ApJ, 804, 1

Faigler, S., Mazeh, T., Quinn, S. N., et al. 2012, Seven New Binaries Discovered in the Kepler Light Curves through the BEER Method Confirmed by Radial-velocity Observations, ApJ, 746, 185

Gelino, D. M. & Kane, S. R. 2014, Phase Curves of the Kepler-11 Multi-planet System, ApJ, 787, 105

Gillon, M., Triaud, A. H., Demory, B. O., et al. 2017, Seven Temperate Terrestrial Planets around the Nearby Ultracool Dwarf Star TRAPPIST-1, Nature, 542, 456

Hamers, A. S., Antonini, F., Lithwick, Y., et al. 2017, Secular Dynamics of Multiplanet Systems: Implications for the Formation of Hot and Warm Jupiters via High-eccentricity Migration, MNRAS, 464, 688

Hills, J. G. & Dale, T. M. 1974, The Orbit Evolution of the Eclipsing Binary System BD +16 516 and the Rotation Period of its White Dwarf, A&A, 30, 135

Hippke, M. & Angerhausen, D. 2015, Photometrys Bright Future: Detecting Solar System Analogs with Future Space Telescopes, ApJ, 810, 29

de Pater, I., Lissauer, J.J., & Hubbard, W.B. 2002, Planetary Sciences, Phys. Today, 55, 64

Jurić, M. & Tremaine, S. 2008, Dynamical Origin of Extrasolar Planet Eccentricity Distribution, ApJ, 686, 603

Laskar, J., Bou, G., & Correia, A. C. 2012, Tidal Dissipation in Multi-planet Systems and Constraints on Orbit Fitting, A&A, 538, A105

Limbach, M. A. & Turner, E. L. 2015, Exoplanet Orbital Eccentricity: Multiplicity Relation and the Solar System, PNAS, 112, 20

Lissauer, J. J., Marcy, G. W., Rowe, J. F., et al. 2012, Almost All of Kepler's Multiple-planet Candidates are Planets, ApJ, 750, 112

Loeb, A. & Gaudi, B. S. 2003, Periodic Flux Variability of Stars Due to the Reflex Doppler Effect Induced by Planetary Companions, ApJL, 588, L117

Lovis, C., Ségransan, D., Mayor, M., et al. 2011, The HARPS Search for Southern Extra-solar Planets – XXVIII. Up to Seven Planets Orbiting HD 10180: Probing the Architecture of Low-mass Planetary Systems, A&A, 528, A112

Mayor, M. & Queloz, D. 1995, A Jupiter-mass Companion to a Solar-type Star, Nature, 378, 355

Mazeh, T., Nachmani, G., Sokol, G., et al. 2012, Kepler KOI-13.01 – Detection of Beaming and Ellipsoidal Modulations Pointing to a Massive Hot Jupiter, A&A, 541, A56

Rauer, H., Catala, C., Aerts, C., et al. 2014, The PLATO 2.0 Mission, Exp. Astron., 38, 249

Ricker, G. R., Winn, J. N., Vanderspek, R., et al. 2014, Transiting Exoplanet Survey Satellite, J. Astron. Telesc. Instrum. Syst., 1, 014003

Rybicki, G. B. & Lightman, A. P. 2008, Radiative Processes in Astrophysics (Hoboken, NJ: Wiley & Sons)

Schmitt, J. R., Wang, J., Fischer, D. A., et al. 2014, Planet Hunters. VI. An independent Characterization of KOI-351 and Several Long Period Planet Candidates from the Kepler Archival Data, AJ, 148, 28

Seager, S. & Hui, L. 2002, Constraining the Rotation Rate of Transiting Extrasolar Planets by Oblateness Measurements, ApJ, 574, 1004

Serrano, L. M., Barros, S. C. C., Oshagh, M., et al. 2018, Distinguishing the Albedo of Exoplanets from Stellar Activity, A&A, 611, A8

Shallue, C. J. & Vanderburg, A. 2018, Identifying Exoplanets with Deep Learning: A Five-planet Resonant Chain around Kepler-80 and an Eighth Planet around Kepler-90, AJ, 155, 94

Tremaine, S. & Zakamska, N. L. 2004, Extrasolar Planet Orbits and Eccentricities, AIP Conf. Proc., 713, 243

Tuomi, M. 2012, Evidence for Nine Planets in the HD 10180 System, A&A, 543, A52

Welsh, W. F., Orosz, J. A., Seager, S., et al. 2010, The Discovery of Ellipsoidal Variations in the Kepler Light Curve of HAT-P-7, ApJL, 713, L145

Yu, Q. & Tremaine, S. 2001, Resonant Capture by Inward-migrating Planets, AJ, 121, 1736

Zinzi, A. & Turrini, D. 2017, Anti-correlation Between Multiplicity and Orbital Properties in Exoplanetary Systems as a Possible Record of their Dynamical Histories, A&A, 605, L4

Zucker, S., Mazeh, T. & Alexander, T. 2007, Beaming Binaries: A New Observational Category of Photometric Binary Stars, ApJ, 670, 1326